Article:
Hernandez-Nava, E., Smith, C.J., Derguti, F. et al. (2015) The effect of density and feature size on mechanical properties of isostructural metaffic foams produced by additive manufacturing. Acta Materialia, 85. 387 - 395. ISSN: 1359-6454

https://doi.org/10.1016/j.actamat.2014.10.058

The effect of density and feature size on mechanical properties of iso-structural porous metals produced by additive manufacturing

E Hernandez-Nava[a,*], C.J. Smith[a], F Derguti[a], S Tammas-Williams[b], F Leonard[b], P.J. Withers[b], I Todd[a], R Goodall[a]

[a]*Department of Material Science & Engineering, The University of Sheffield, Sir Robert Hadfield Building, Mappin St, Sheffield S1 3JD, UK*
[b]*Henry Moseley X-ray Imaging Facility, School of Materials, The University of Manchester, M13 9PL, UK.*
*Corresponding author. Tel. +44 1142225988. E-mail address: mtq10eh@sheffield.ac.uk

Abstract

Simple models describing the relationship between basic mechanical properties and the density of various types of porous metals (such as foams, sponges and lattices) are well established. Carefully evaluating these relationships experimentally is challenging however, because of the stochastic structure of foams and the fact that it is difficult to systematically isolate density changes from other variations, such as in pore size and pore position. Here a new method for producing systematic sets of stochastic foams is employed based on Electron Beam Melting (EBM) additive manufacturing (AM). To create idealised structures, structural blueprints were reverse engineered by inverting X-ray computed tomographs (XCT) of a randomly packed bed of glass beads. This 3D structure was then modified by computer to create five foams of different relative density ρ_r but otherwise consistent structure. Yield strength and Young's modulus have been evaluated in compression tests and compared to existing models for foams. A power 3 rather than a squared dependence of stiffness on relative density is found, which agrees with a recent model derived for replicated foams. Further analysis of the strength of the parent metal and idealised nominally fully dense rods of different diameters showed a decrease in strength with decreasing dimensions. The results

suggest that surface defects means the minimum size of features that can be created by EBM with similar strength to machined samples is around 1mm.

Keywords: Metal foam; cellular solids, reverse engineering**,** open-cell foam; X-ray computed tomography

I. Introduction

Metallic foams have been the subject of many investigations, due to their potential performance in a wide range of application areas [1]; exploiting interesting mechanical [2][3], thermal [4], electrical [5][6] and acoustic [7] properties. Foam properties can be tailored within certain ranges to suit particular applications, for example by varying the relative density, ρ_r defined as the ratio of foam density to fully dense solid. Several models exist allowing the effect this has on the mechanical properties to be estimated; the most generally applicable and widely used being the equations of Gibson and Ashby [3], which are based on the definition of a simple cubic unit cell and the use of beam theory to predict the response to load. Examples of the equations for elastic modulus (E) and strength (σ) are given below:

$$\frac{E^*}{E_s} = C_1 \rho_r^2 \quad (1)$$

$$\frac{\sigma^*}{\sigma_s} = C_2 \rho_r^{3/2} \quad (2a)$$

$$\frac{\sigma^*}{\sigma_s} = C_2 \rho_r^{3/2} \left(1 + (\rho_r)^{1/2}\right) \quad (2b)$$

where the terms with a superscript * relate to the foam and those with a subscript *s* relate to the constituent metal and C_1 and C_2 are constants of proportionality. The second bracketed term in equation 2b is a density correction term for foams having a relative density greater than 0.3 [2].

While such equations are often preferred for their simplicity and capability to capture broad trends in foam response, they are not always accurate for specific types of foam. In cases where the equations are not followed, it is often not easy to determine the cause, although this is usually interpreted as a departure from the beam-bending mechanisms that underlie equations (1-3) [8].

For foams where disparities arise it is often the case that the exponent relating density to Young's modulus is found to be bigger or smaller than 2. The fact that an exponent of 2 would be expected in the general case, even for more complex structures than that considered in the Gibson-Ashby analysis and is supported by the results of Rossoll and Mortensen [9], who used finite element simulations of 7 strut building blocks representative of certain foam structures (gas injection [10], replication [11]) to explore the expected variation in elastic response with density. For most of the density range considered in this modelling study an exponent of 2 was found to give a good match. A drop off in relative modulus was observed for a tapered structure representing replicated foams only below a relative density of 0.03, which in practice is not encountered in these materials.

There are, however, specific cases that produce notable departures from this rule. For example, it is often observed experimentally that foams processed by replication are better described by an exponent close to 3 in equation (1). This has been explained by Mortensen et al. [12] as being due to changes in the architecture of the foam with density (i.e. the geometrical structure of the foam is not density independent). The derivation underlying this considers a structure formed of interpenetrating spheres (the pores) and decreases the foam density by bringing their centres closer together. As an alternative to the Gibson-Ashby structure, in this case the foam is more accurately

described as consisting of relatively thin struts and rather thicker nodes where the struts interconnect [13]. This brings in a number of additional factors which are considered in the derivation; (i) if beams are considered to deform by bending, then it is the thinnest regions of the struts that will dominate the behaviour [14], (ii) a change in foam density results in a change in both the shape of the connecting struts and the number of struts that meet at nodes, (iii) there will be a distribution of strut sizes, with the larger struts defined in initial packing of particles having a dominant effect, (iv) there is a point, reached at a finite relative density $\rho_{r,c}$ (following the notation used here; this value is taken to be 5% in Ref. [12]), where, although there is still material present, the structure ceases to be integrated and able to bear load. It is predicted that the elastic response of such a foam will follow the equation below, which is found to produce a consistent slope with density variations with data from replicated foams:

$$\frac{E^*}{E_S} = \frac{\left(1-2\left(\frac{1-\rho_r}{1-\rho_{r,c}}\right)^{2/3}+\left(\frac{1-\rho_r}{1-\rho_{r,c}}\right)^{4/3}\right)}{\left(1-2\left(\frac{1-\rho_{r,0}}{1-\rho_{r,c}}\right)^{2/3}+\left(\frac{1-\rho_{r,0}}{1-\rho_{r,c}}\right)^{4/3}\right)} \quad (3)$$

where all terms are as defined previously, with $\rho_{r,0}$ the initial packing fraction of a powder, typically 0.36 for random packing.

Direct experimental investigation of such relationships are not easy to perform because most methods for manufacturing porous metals do not allow systematic definition of density and pore shape, pore location, etc, so as to systematically determine the influence of each of these factors. The topological structure will be strongly influenced by the processing route, the choice of which is often limited by the parent material [15].

To isolate and analyse the effect of density alone on foam properties one needs a highly controllable manufacturing method.

Additive Manufacturing (AM) has recently emerged as a fabrication route for complex 3D parts. In such methods the object is built up by the addition of thin layers of material on top of each other, guided by a stereo lithography (STL) file. This file which is the geometrical blueprint for the manufactured object can be defined by CAD or input from 3D measurements thereby creating a clone of an original object. Electron Beam Melting (EBM) is an AM technique that has shown to be particularly well suited to the manufacturing of complex architectures, and in particular porous metals in the form of regular lattices [16][17]. Typically, it has been employed for biomedical porous implants [18] and impact energy absorbing materials in the form of both stochastic and non-stochastic structures [19].In the present study, we have been able to systematically investigate the relationship between foam density and mechanical properties of porous metals to examine the predictive capability of foam models. This has been done by coupling EBM manufacture of titanium foams using. This stochastic baseline structure was modified in the computer to define a systematic set of foam samples for manufacture and mechanical characterisation.

II. Experimental procedure

2.1 X-ray Computed Tomography

2.1.1 Scanning Process

XCT was carried out at the Henry Mosley X-ray Imaging Facility on a Nikon Metrology 225/320 kV Custom Bay system. First, a 56.5mm diameter cylindrical plastic container was scanned filled with glass spheres of 3.9 mm in diameter to a depth

of approximately 35 mm, no vibration was used such that the spheres were located where they fell. Second, a set of seven 'fully' dense additively manufactured rods were scanned each having a different diameter (table 1). An accelerating voltage of 160 kV and a 110 µA current were used to produce a white beam of X-rays radiating from a spot of 5 µm from a tungsten target.

The source-sample-detector positions were such that 10x magnified images were collected on a Perkin Elmer 2048×2048pixel 16-bit amorphous silicon flat panel detector having a pixel size of 200µm giving an effective pixel size of 20µm. The sample was rotated through 360 degrees and a total of 3142 radiographs taken using the Nikon-Metrology Inspect-X acquisition software.

2.1.2 Data processing

The 2D radiographs were computationally reconstructed into a 3D volume, figure 1 using Nikon-Metrology's CT-pro software based on a filtered back-projection algorithm. The volume was reduced from 16-bit to 8-bit using VGStudio MAX in order to allow the data to be processed and visualised.

The data was loaded into Avizo 7.1 and then cropped to include only the glass spheres and pore spaces. Two threshold values were chosen to segment the images giving two air/glass ratios. These images were inverted such that the pore spaces became the struts of the foam and the glass regions the pores. Finally the two 3D structures were exported to ScanIP software to produce STL files for the additive manufacturing process.

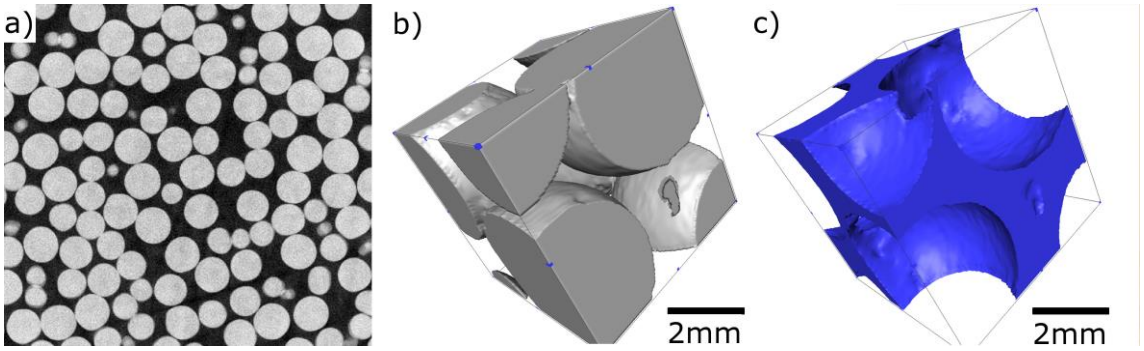

Fig. 1. (a) A region taken from a 2D virtual slice through the 3D CT image of the 3.9mm spheres (b) segmented 3D representation of a small part of the 3D image, (c) inverted image showing the spheres as cavities within a solid framework; this gave the baseline 3D geometry file for the manufactured porous foams.

2.2 Foam STL modification

The STL files were modified using Magics 16©, a rapid prototyping software in order to produce a systematic set of foams. The surface defining the volume was modified through a series of offset operations from the baseline image in figure 2a by dilating or contracting the boundaries in units of 100 µm. Figure 2b shows the boundaries of all five samples.

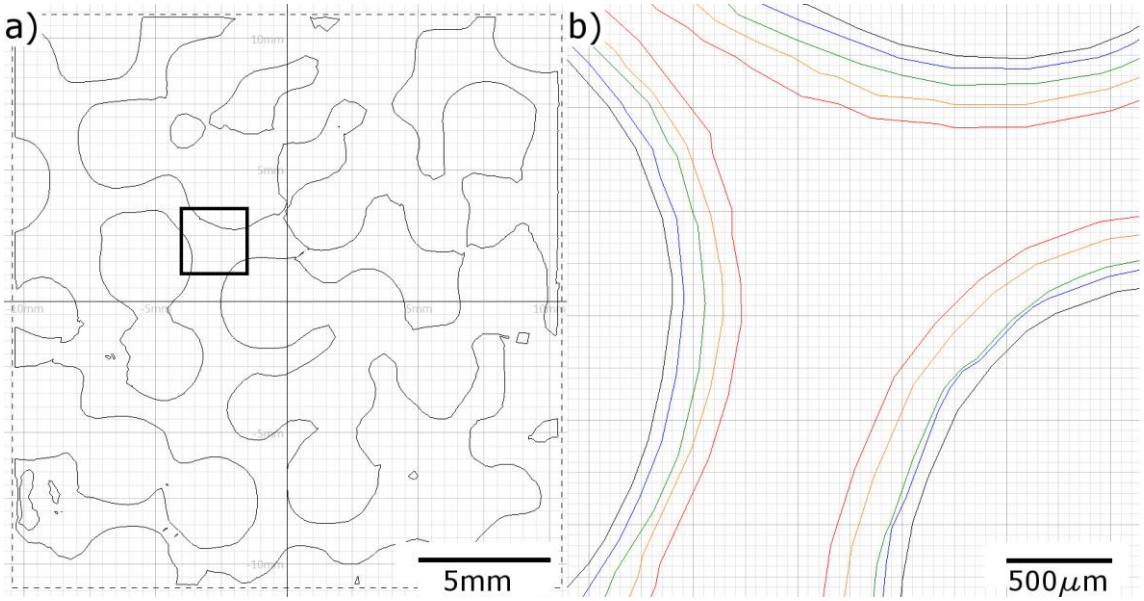

Fig. 2.a) 2D cross section of the inverted bead pack b) a node in the STL files used showing the difference in thickness produced by a surface offset of 100µm. It should be noted that the boundary spacing is not shown uniformly for all cases, due to triangle distortion in the STL file. Relative density of each sample is shown.

A total of five foam blueprints each having different relative densities but the same architectural features were obtained. 2×2×3.5cm volumes of interest were extracted from the 3D models to manufacture samples of these dimensions for compression testing under quasi static conditions. The cropping of the 3D image to this size ensured a minimum of 5-9 pores across each direction, respecting the minimum necessary number of pores required to representative of a material [20].

2.3 EBM manufacturing

A total of 15 samples (three each of the 5 densities) were manufactured using an ARCAM EBM S12 machine from Ti-6Al-4V prealloyed powder having 45-100 µm particle size as the raw material. All foam samples were fabricated in one build operation in order to avoid differences in chemical composition from recycled powder [21].

The electron beam processing was carried out with 102W in beam power (produced from 60kV accelerating voltage and 1.7mA beam current), scanning the focussed beam at 200m/s. After manufacture they were removed from the EBM machine, and compressed air was used several times to remove loose powder from the pores in all foams. An example of each of the 5 structures is shown in figure 3. All samples were weighed and measured with callipers so that the relative density could be obtained.

In addition, a set of 21 individual 'fully' cylindrical dense rods were manufactured for flexural strength tests and X-ray tomography investigation, to assess the influence of "as built" features e.g. porosity and surface roughness on the strut strength. These were 80mm long having diameters as summarised in table 1.

2.4 Mechanical tests

All foam samples were compressed in a Hounsfield universal test rig TX0039 at room temperature and at an initial strain rate of 2×10^{-4} s^{-1}. Stress-strain histories could be obtained from the load displacement curves after correcting for the test rig compliance, which was done using compressive cycles up to the highest tested load with no sample present between the compression platens.

Many samples showed a small region of exponential load increase before the linear elastic portion of the curve was reached. This is characteristic of many foam tests and is attributed to non-instantaneous contact between machine platen and the full faces of the test samples giving an effective misalignment[22]. This was corrected for by a small shift in strain values following the procedure detailed in [23].

The curves were used to determine the Young's modulus from the gradient of the linear elastic portion of the curve, the 0.1% offset yield strength and the compressive resistance, table 1 (taken as the maximum point on the curve before the first decrease as the structure collapses).

Additionally, in order to characterize the change in material properties as a function of additively manufactured feature size (test-piece diameter), three point bending tests were carried out on fully dense rods using a Zwick/Roell Z050 machine with a 5kN load cell. A constant strain rate ($2.2\times10^{-3} \pm 3.5\times10^{-4}$ /s) according the standard ASTM

C1684-13 and span-to-depth ratio of 36 were used. Flexural 0.1% Yield strength has been extracted in a similar fashion as for compression tests following the equations 4 and 5.

$$\sigma_{flex} = \frac{8PL}{\pi\phi^3} \tag{4}$$

$$\varepsilon_{flex} = \frac{6\delta d}{L^2} \tag{5}$$

where P, L, ϕ, δ and d are: the load, span length and rod diameter, maximum deflection of the centre of the beam and d the depth of the tested beam.

The microhardness was mapped across these samples using a square array of Vickers indents from an automated Struers Durascan 70 hardness on polished cross sections.

III. Results and analysis

3.1 Relative density

As previously stated, the space recorded between the glass beads using XCT was used as the design for the AM foam. The glass spheres, randomly distributed, worked as nodal points within the foam such as spacers, possibly not equally positioned throughout the entire volume. This process should be analogous to the structural formation that takes place in foams processed by the replication method [24].

The relative densities for all samples were measured and are reported in table 1. Good reproduction of the designed forms was found. A 7%±1% difference in relative density between consecutive samples was achieved with a 100µm offset and the chosen threshold values from the XCT data processing.

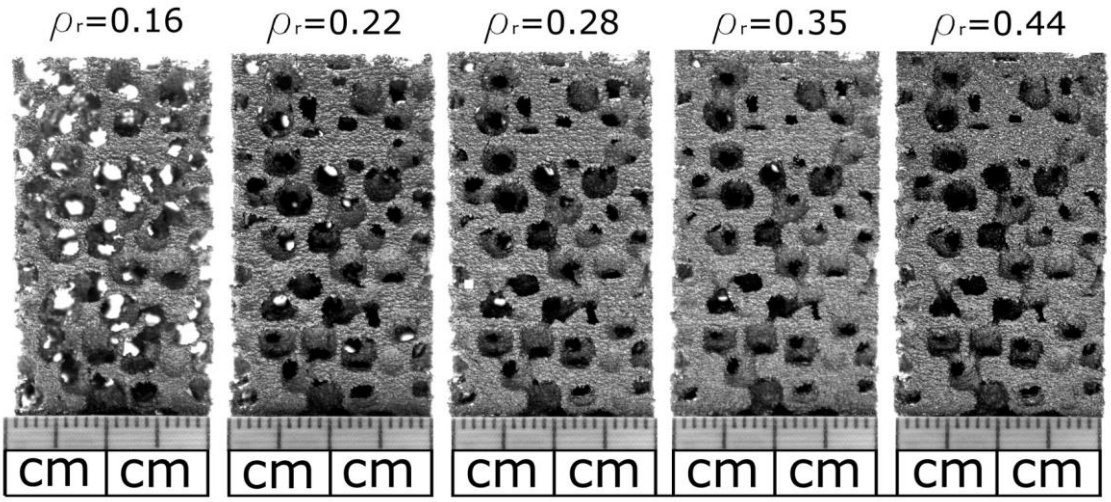

Fig. 3. Foam samples produced by XCT and EBM, with the measured relative density shown.

Table 1.Mean properties of the 5 fabricated foam sample sets and corresponding single rod samples after the compression and bending tests

Foam samples						***Dense rod samples***			
File btained hrough	***Relative density, (ρ_r)***		***Young's Modulus (GPa)***	***0.1% offset yield strength (MPa)***	***Peak Compressive resistance σ^* (MPa)***	***Diameter (mm)***	***Micro Vickers Hardness***	***Porosity volume fraction***	
	File	***Measured***							
STL	0.13±7x10^{-3}	0.16±4x10^{-3}	*0.65±0.05*	*7.72±0.57*	*11.7 ± 3.6*	*0.56*	*391±12.8*	*0.028*	
XCT	0.20±6x10^{-3}	0.24±6x10^{-3}	*1.79±0.15*	*29.7±3.1*	*35.0 ± 4.6*	*0.75*	*366±17.3*	*0.070*	
XCT	0.26±7x10^{-3}	0.28±6x10^{-3}	*3.19±0.21*	*48.3±5.3*	*56.7 ± 9.1*	*0.97*	*386±21.3*	*0.019*	
STL	0.33±7x10^{-3}	0.35±7x10^{-3}	*5.63±0.36*	*88.7±7.4*	*102.7 ± 10.9*	*1.13*	*375±15.5*	*0.029*	
STL	0.40±7x10^{-3}	0.44±5x10^{-3}	*10.92±0.41*	*119.4±5.8*	*156.9 ± 9.4*	*1.43*	*377±17.6*	*0.009*	
						1.71	*381±19.4*	*0.029*	
						1.90	*382±19.4*	*0.037*	

3.2 Compressive response

A typical example of a stress-strain curve for compression of a sample of relative density 0.16 is shown in figure 4. In virtually all cases the stress strain curves show the initial linear elastic stage, followed by a post-yielding reduction in stress supported, which was observed experimentally to be coincident with failure of some of the foam struts in a brittle manner. Brittle failure is consistent with the low ductility expected of this alloy.

Upon compression testing, values of Young modulus, 0.1% offset yield strength and peak compressive resistance were obtained, table 1. Variability in the reported values within each set may be due to the intrinsic statistical nature of the experiments, but cannot be attributed to variations in the structure, as the test samples for a given set were identical geometrically. The only such variable that may influence the results are minimal variations in the fabricated cross sectional areas from the processing method, which could be significant under compression due to yielding across weak sections. Additionally, it should be remembered that the samples tested here were made in a single batch to eliminate the effect of reused particles, which otherwise could have an impact on mechanical properties [21].

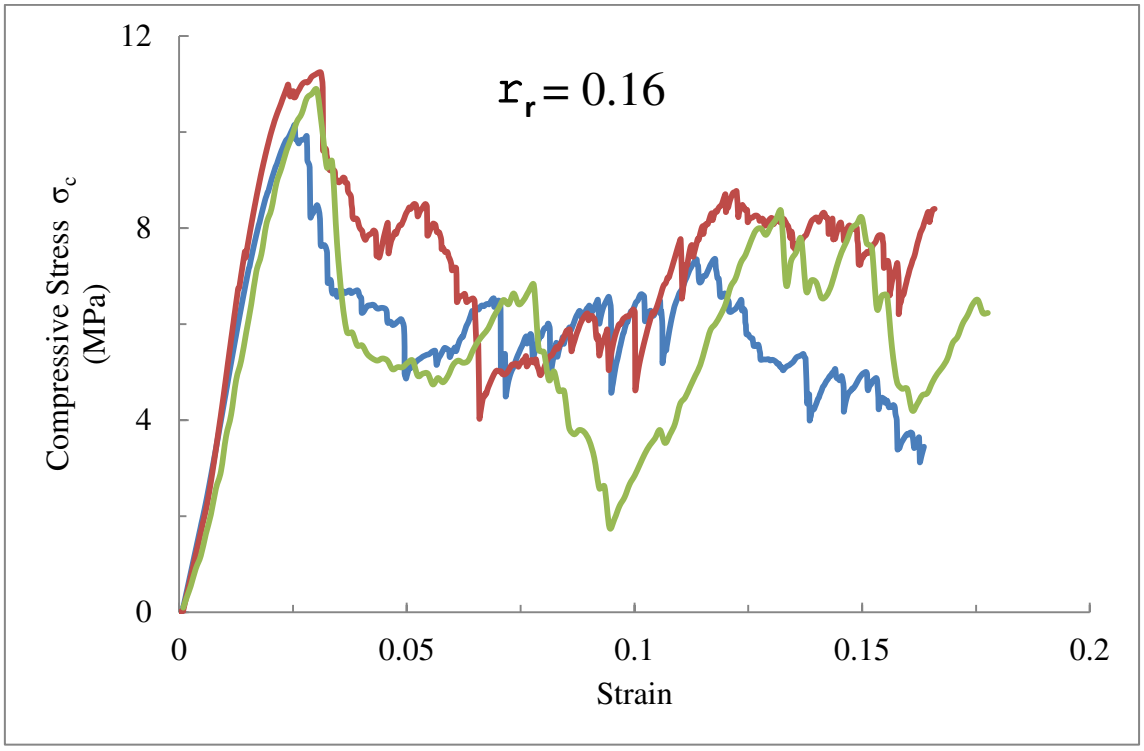

Fig. 4. Engineering stress strain response of the three XCT-AM foam samples at 0.16 relative density.

3.3 Elastic Properties

The variation in elastic properties with density is usually expressed in terms of the Young's modulus relative to that of the fully dense parent metal, E_s. Here a value of 114GPa is taken from tests on 100% dense EBM machined tensile specimens, although in the absence of 3D CT data it is not possible to put a level on the amount of porosity contained within the struts. Some porosity is likely and this will reduce the properties to some extent [25]. Chemical analysis on the employed EBM powder reported a wt% of 6.35 Al, 4.19 V, 0.007 C, 0.15 Fe, 0.121 O, 0.015 N, 0.0015 H and the balance being

titanium.

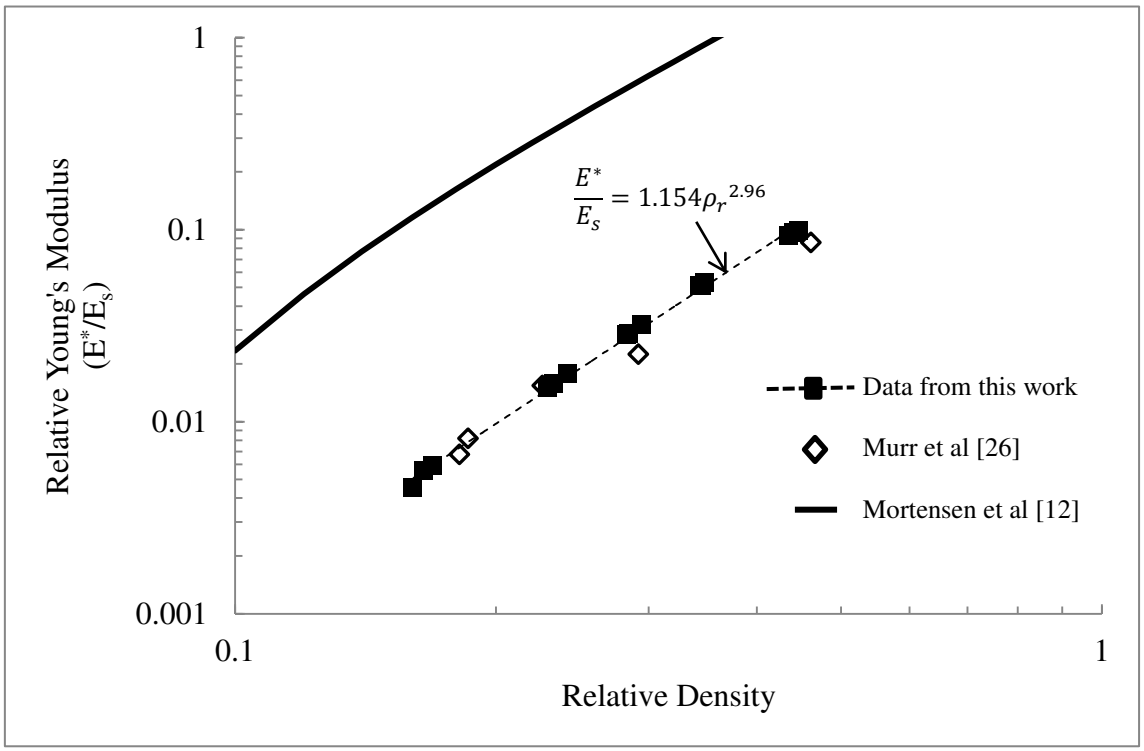

Fig. 5. Relative Young's modulus plotted against relative density for Ti-6Al-4V foams from this work against the prediction from the model of Mortensen et al [12]. Additionally, data points are included for other additively manufactured foams from [26].

These data are plotted against relative density in Figure 5, fitted to by an equation of the form of equation (1), giving a least squares fit with an exponent of 2.96. This is consistent with the range of values predicted by the model developed for replicated foams [12], which can be seen by the matching slope in the graph. This supports the idea that foams processed by replication, where variations in density will produce the same kind of structural variation seen here, will show a higher sensitivity to density than other foam types.

However, even though the replication model captures the trend, it significantly over predicts the absolute values in figure 5. In order to obtain a fit a constant prefactor (a

"knockdown" constant) must be included in equation (4). This is similar to what is often needed with the Gibson-Ashby predictions, where the constant can take a wide range of values. Here a good fit is obtained when a value of 0.053 is used representing a knockdown of 20 times, the low level of which may indicate that the morphology of these foams is still much less efficient than the structure considered in the development of the Mortensen model (this could for example be due to imperfect reproduction of the structure in the additive manufacturing process or redundant members not linking nodes within the solid network, produced after the CAD models were cropped).

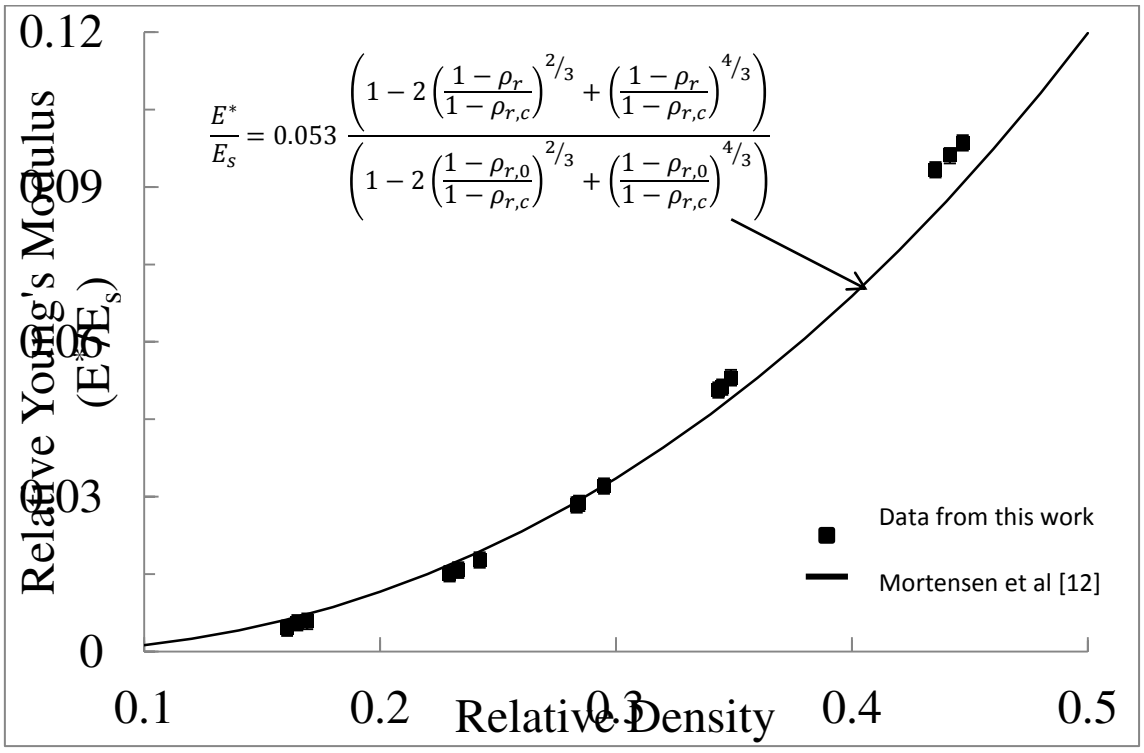

Fig. 6. Relative Young's modulus data matched against the model from Ref. [12], including a knockdown parameter of 0.053. Error bar added representing standard deviation within sample testing

3.4 Compressive strength

As for the elastic response, the strength of foams can be usefully presented in terms of relative strength. Due to microstructural effects, it is less clear what the correct value of

the parent metal strength should be, here σ_s is taken as 848 MPa (the 0.2% yield strength previously obtained from tensile specimens machined from nominally fully dense material in the as-manufactured EBM condition).

Figure 7 plots the relative yield strength determined for the foams tested here against relative density. Fitting the data to an equation of the form expressed by equation (2a) gives a relationship with a constant (C_2) of 1.67 and an exponent of 2.81. Although the yield strength of foams has not always been well defined in the literature, here in table 1, the previous values have been obtained from the 0.1% yield strength on stress-strain curves.

Both constants are somewhat different from those that would normally be expected for foams [27]. However, these relationships are indicative only, and the expressions are not followed precisely by all foams. Few data have been reported so far on compression resistance on these type of foams, however, some previous EBM titanium foams that have been investigated are reported to follow the predictions of equations (2a) and (2b) (depending on the density) [28]. For comparison the best fits obtained by these equations separately (i.e. not requiring that they are continuous across a relative density of 0.3) are also shown in Figure 7. It is noteworthy that recent studies on Ti-6Al-4V foams processed by a spherical space holder method (and therefore with a similar topology to the foams considered here) and similar levels of porosity show comparable values; an exponent of 2.28 and a constant of proportionality of 1.07 [29].

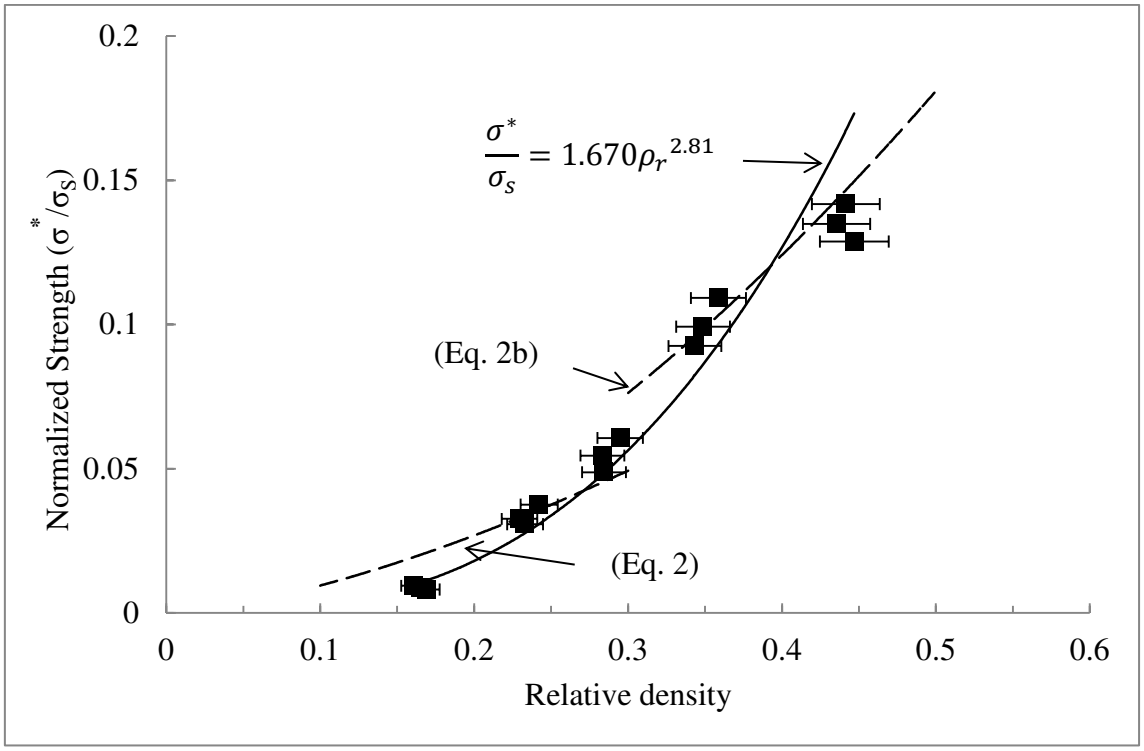

Fig. 7. Compressive resistance against relative density of the Ti-6Al-4V foam. Multiple fits can be observed from equations 2a and b from the reported literature [2]. Error bar added representing standard deviation within sample testing.

3.5 Parent metal strength

The mechanical properties of the foams made (the absolute strength values, not the relative strengths that were plotted in Figure 7) can be further used to analyse the resistance to plastic deformation of the constituent metal. This is done following the theory of porous metal deformation of Ref. [8], based on a modified secant modulus method to predict the plastic flow stress. The procedure used is outlined in [30]. In essence a function is found that links Young's modulus of the foam to that of the parent metal:

$$E^* = F(\rho_r).E_s \quad (6)$$

This function is used as a measure of the load bearing efficiency of the foam structure. It is further assumed that the metal making up the foam (and thus the foam itself) undergoes plastic deformation according to a Holloman power law:

$$\sigma = c\varepsilon^{n} \tag{7}$$

where *c* and *n* are constants. The method of [8] predicts that the foam will thus deform plastically according to:

$$\sigma_f = C\varepsilon^n \quad \text{with} \quad \frac{C}{c} = F^{\frac{1+n}{2}}\rho_r^{\frac{1-n}{2}} \tag{8}$$

where σ_f is the stress the foam will support at a certain value of strain, ε_f, and other terms are as defined previously. This allows the flow stress of the metal to be estimated from foam strength data, when all relevant parameters are known.

Here, the value of *n* is determined from the foam data, as this is predicted to be the same as that for the bulk metal. The curves for the highest density foams are used, as these give a large strain before the first cell collapse event that results in a stress drop. Fitting a curve of the form of equation (7) to the initial plastic deformation part of these curves produces an average value of $n = 0.124$. The function *F* can be taken as the least squares equation expressing how the relative modulus varies with density, in this case:

$$F(\rho_r) = 1.154\rho_r^{2.96} \tag{9}$$

Substituting this into equation (8) with the value of *n* determined allows an expression to determine σ (for the metal at an equivalent strain) to be found from σ_f. Using this on the samples tested produces the results in figure 8.

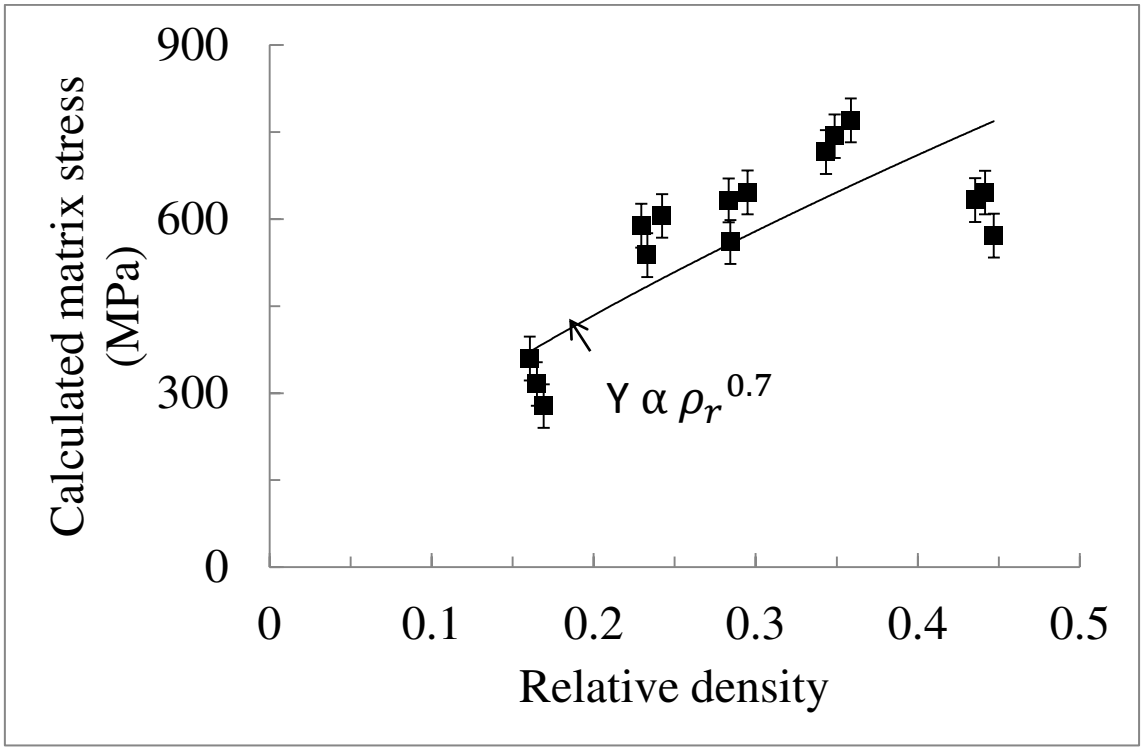

Fig. 8 – the variation in parent metal flow stress, extracted from each of the five sets of three foam samples tested for each condition, with foam relative density. Error bar added representing standard deviation within sample testing.

This shows that, if this model is correct, there is an appreciable increase in parent metal flow stress with sample relative density, up to at least a value of around 0.35. The lower value found at higher relative densities than this may indicate that the matrix strength is casing to vary, or, as these foams are high density, it may rather indicate that the mechanism of deformation is changing to involve yielding rather than bending [2]. In these circumstances, the behaviour of the foam may depart from a uniform mode that underlies the assumptions of the method. A small degree of variability in the results can be observed in each group of relative density possibly to a different response from foam to foam.

The large change in the strength of the metal (remembering that any changes due to the different levels of porosity are expected to have been removed by the analysis) may be explained by the changing number, distribution or effect of microstructural features or defects inside the deposited material with size of part. Isolating the effect of each of these possibilities, and discriminating between possible strengthening mechanisms, such as phase transformation or texture effects, and detrimental effects from volumetric defects (internal porosity and/or surface roughness) is complex, and to provide more data tests without the geometrical complexity of the foam samples are required.

3.6 Fully dense rod testing

In order to investigate the influence of additively manufactured strut dimensions on strength, three point bending tests have been carried out on nominally fully dense test pieces and the results are plotted in figure 9. Given that the yield stress of Ti-6Al-4V is normally between 900 and 1000MPa this shows that good strengths are achieved at

scales greater than around 1mm.

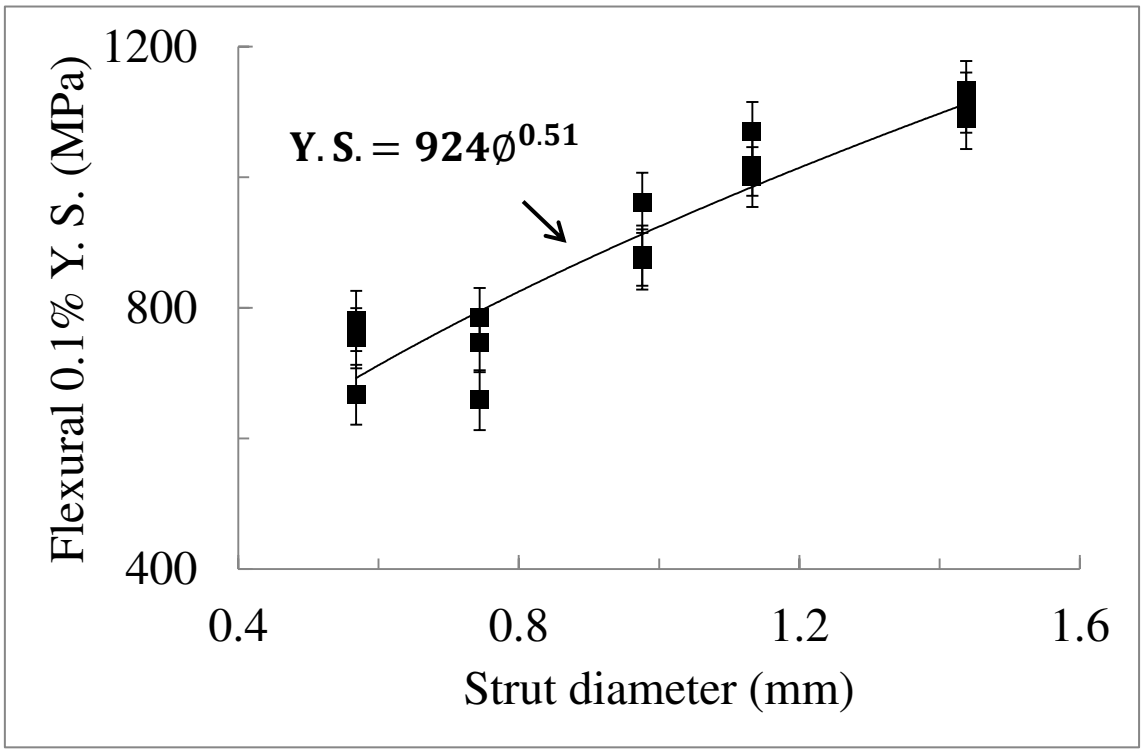

Fig. 9. Flexural 0.1% yield strength as a function of diameter of nominally fully dense cylindrical rods made by EBM. Error bar added representing standard deviation within sample testing.

It is clear from Figure 9 that there is a decrease in yield strength measured in bending as the rod diameter becomes smaller. This trend, though not the absolute values, is consistent with the results of Figure 8 estimated from the foam responses. Further analysis on the rod samples was performed to look at some of the possible causes.

Figure 10a shows the variation in porosity within the rods, as determined by X-ray tomography. It can be seen that apart from one relatively high value of porosity at a relatively low value of rod diameter (which appears to be an isolated result) the level is roughly consistent over all rod diameters, and no systematic variation is seen, meaning that increased porosity at small feature sizes cannot explain the variation.

An alternative explanation would be a change in microstructure due to the higher cooling rates associated with fabricating smaller features. To explore this, cross-sectional metallography has been taken, and the polished cross sections have also been mapped with microhardness tests (Figure 10b-g). The micrographs show a slightly finer Widmanstätten α+β microstructure in the case of thinner rods, as would be expected for higher cooling rate. However, the microhardness maps do not indicate any systematic variation in hardness with location, and the average hardness values for each sample are consistent, Table 1. Therefore, while microstructural variations (or indeed texture effects which have not been examined) cannot be completely dismissed as a possible cause for the decrease in strength at small diameters this seem implausible.

The presence of surface stress concentrations at the surface, e.g. notches and cracks are likely to lower the strength of the struts. This means that, if the likelihood of surface defects and the scale of surface roughness is the same irrespective of sample dimensions, the effect on the strength will become more significant for thin struts. From the X-ray computed tomography scans of the rods shown in Figure 10h-j the scale of the surface roughness remains comparable (of the order of 100 μm) as the rod diameter is changed. It is therefore suggested that, of the possible contributors to the decrease in strength at smaller diameters, this is likely to be the most significant.

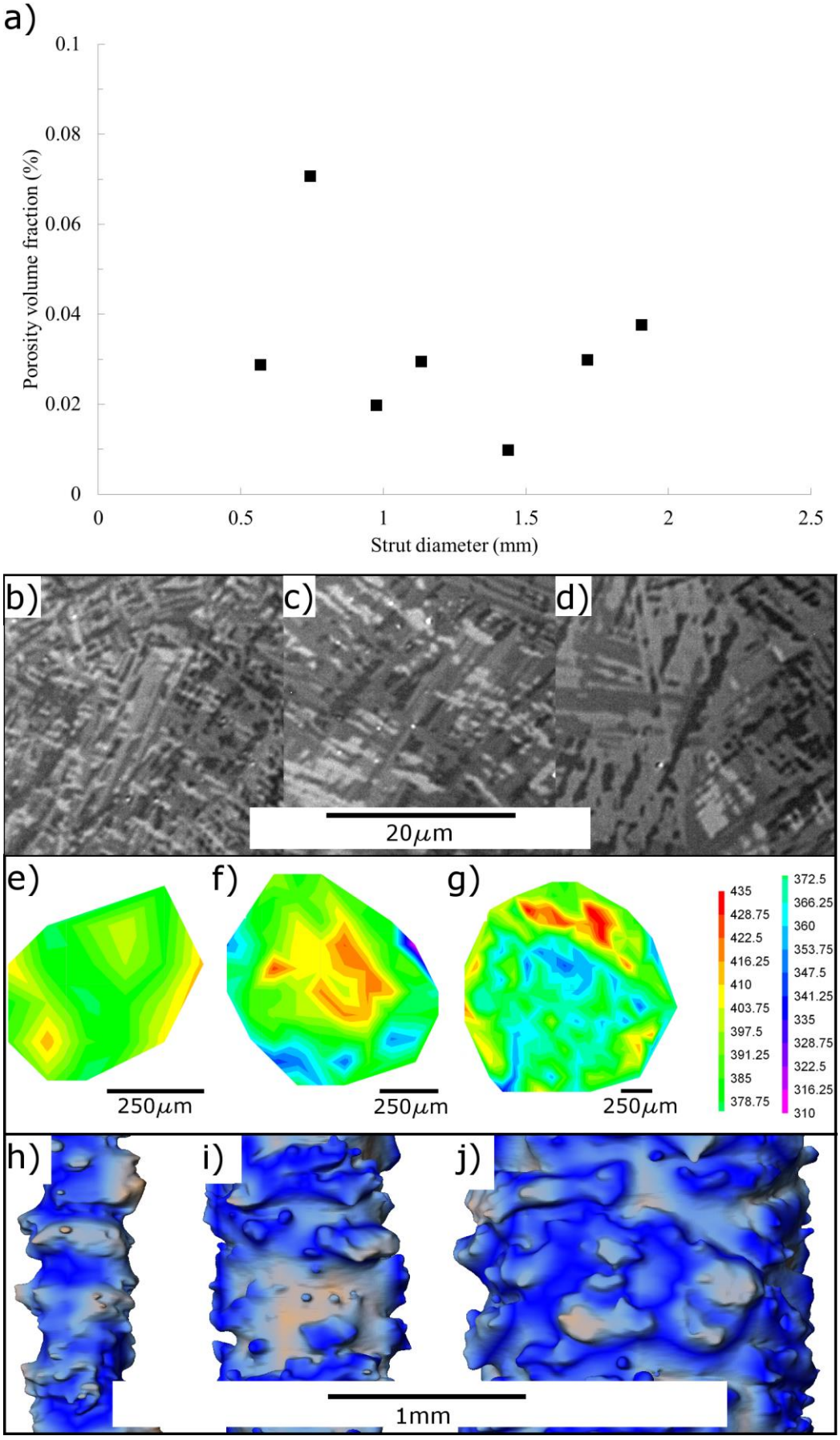
a)
Porosity volume fraction (%)
0.1
0.08
0.06
0.04
0.02
0
0
0.5
1
1.5
2
2.5
Strut diameter (mm)
b)
c)
d)
20μm
e)
f)
g)
435
428.75
422.5
416.25
410
403.75
397.5
391.25
385
378.75
372.5
366.25
360
353.75
347.5
341.25
335
328.75
322.5
316.25
310
250μm
250μm
250μm
h)
i)
j)
1mm

Figure 10. “As manufactured” characteristics for nominally dense Ti-6Al-4V rods a) internaxl porosity volume fraction obtained from CT scan. Figures b), c) and d) are showing a very fine Widmanstätten α+β microstructure within samples of 0.56, 0.744 and 1.8mm diameter. Figures e), f) and g) showing microhardness Vickers maps of same samples respectively. Figures h), i) and j) showing the surface roughness obtained from CT scans.

IV. Conclusions

A 3D model of a porous material with stochastic structure and uniform pore size was obtained by imaging a random array of glass spheres using X-ray Computed Tomography. This was used as a template for the production of 5 stochastic foams having the same geometries and pore arrangements but thicker walls (and hence higher density), thereby allowing the effect of this variable on the strength of foams to be systematically investigated.

When additively manufactured in Ti-6Al-4V by EBM these samples were found to display a variation in Young’s modulus which was different from that predicted by the ideal case of Gibson-Ashby in that the exponent connecting stiffness to relative density was not of order 2 but 3. This exponent has been predicted by Mortensen et al. [12] and has been explained to be the result of the structures being relatively highly susceptible to changes in density.

The yield strength of the foams was also found to increase approximately as the third power of the density. For strength, the variation against relative density was found to be in accord with previous results on materials with similar structures processed by other means. An alternative model developed for replication processed foams captures the trend and shows good correlation with the data on elastic properties reported here, provided a knockdown factor of around 20 is used. This is a large decrease in the properties from that predicted, even though this factor can cover a wide range, and is

likely to be due to the foam structure produced being very inefficient, with a large amount of material concentrated in the nodes where struts meet, adding mass but contributing relatively little to the strength. By the application of a modified secant modulus model the yield stress for the parent metal was deduced for each foam and the results indicate an increase in yield stress with strut dimensions, at least for fine struts.

Further investigation through the measurement of flexural yield stress on nominally fully dense additively manufactured rods show a similar fall in yield stress as the diameter was reduced. It is speculated that this is likely to be due to the effect of the surface roughness of material processed by EBM. This suggests that, in order to retain parent material strength values (as in here from tensile test machined EBM samples), the section size of components should be kept above a minimum value in the region of 1mm.

Acknowledgments

One of the authors (E. Hernandez-Nava) would like to acknowledge the support of a studentship provided by CONACyT.

The Manchester X-ray Imaging Facility was funded in part by the EPSRC (grants EP/F007906/1, EP/F001452/1 and EP/I02249X/1

References

[1] R. Goodall and A. Mortensen, “Porous metals,” in *Physical Metallurgy*, 5th ed., vol. 7, D. Laughlin and K. Hono, Eds. Elsevier, in print.

[2] L. J. Gibson and M. F. Ashby, *Cellular Solids Structure and Properties*. Cambridge, 1997.

[3] M. F. Ashby, “The properties of foams and lattices.,” *Philos. Trans. A. Math. Phys. Eng. Sci.*, vol. 364, no. 1838, pp. 15–30, Jan. 2006.

[4] F. Diologent, E. Combaz, V. Laporte, R. Goodall, L. Weber, F. Duc, and A. Mortensen, “Processing of Ag–Cu alloy foam by the replication process,” *Scr. Mater.*, vol. 61, no. 4, pp. 351–354, Aug. 2009.

[5] K. S. Challagulla and T. A. Venkatesh, “Electromechanical response of piezoelectric foams,” *Acta Mater.*, vol. 60, no. 5, pp. 2111–2127, Mar. 2012.

[6] R. Goodall, L. Weber, and A. Mortensen, “The electrical conductivity of microcellular metals The electrical conductivity of microcellular metals,” *J. Appl. Phys.*, vol. 044912, 2006.

[7] M. A. Navacerrada, P. Fernández, C. Díaz, and A. Pedrero, “Thermal and acoustic properties of aluminium foams manufactured by the infiltration process,” *Appl. Acoust.*, vol. 74, no. 4, pp. 496–501, Apr. 2013.

[8] J.-F. Despois, R. Mueller, and A. Mortensen, “Uniaxial deformation of microcellular metals,” *Acta Mater.*, vol. 54, pp. 4129–4142, 2006.

[9] A. Rossoll and A. Mortensen, “On the load-bearing efficiency of open-cell foams: A comparison of two architectures related to two processes,” *Scr. Mater.*, vol. 68, no. 1, pp. 44–49, Jan. 2013.

[10] L. Xingnan and L. Yanxiang, “Prediction of melt residual in batch type gas injection foaming process,” *J. Mater. Process. Technol.*, vol. 212, no. 1, pp. 181–187, Jan. 2012.

[11] T. Abdulla, A. Yerokhin, and R. Goodall, “Effect of Plasma Electrolytic Oxidation coating on the specific strength of open-cell aluminium foams,” *Mater. Des.*, vol. 32, no. 7, pp. 3742–3749, Aug. 2011.

[12] A. Mortensen, Y. Conde, A. Rossoll, and C. San Marchi, “Scaling of conductivity and Young’s modulus in replicated microcellular materials,” *J. Mater. Sci.*, vol. 48, no. 23, pp. 8140–8146, Aug. 2013.

[13] C. San Marchi and A. Mortensen, “Deformation of Open-cell aluminium foam,” *Acta Mater.*, vol. 49, pp. 3959–3969, 2001.

[14] R. Goodall, J. Despois, A. Marmottant, L. Salvo, and A. Mortensen, “The effect of preform processing on replicated aluminium foam structure and mechanical properties,” *Scr. Mater.*, vol. 54, pp. 2069–2073, 2006.

[15] J. Banhart, “Manufacture, characterisation and application of cellular metals and metal foams,” *Prog. Mater. Sci.*, vol. 46, no. 6, pp. 559–632, Jan. 2001.

[16] J. Parthasarathy, B. Starly, S. Raman, and A. Christensen, “Mechanical evaluation of porous titanium (Ti6Al4V) structures with electron beam melting (EBM).,” *J. Mech. Behav. Biomed. Mater.*, vol. 3, no. 3, pp. 249–59, Apr. 2010.

[17] L. Yang, O. Harrysson, H. West, and D. Cormier, “Compressive properties of Ti–6Al–4V auxetic mesh structures made by electron beam melting,” *Acta Mater.*, vol. 60, no. 8, pp. 3370–3379, May 2012.

[18] E. Marin, S. Fusi, M. Pressacco, L. Paussa, and L. Fedrizzi, "Characterization of cellular solids in Ti6Al4V for orthopaedic implant applications: Trabecular titanium.," *J. Mech. Behav. Biomed. Mater.*, vol. 3, no. 5, pp. 373–81, Jul. 2010.

[19] H. N. G. Wadley, "Multifunctional periodic cellular metals.," *Philos. Trans. A. Math. Phys. Eng. Sci.*, vol. 364, no. 1838, pp. 31–68, Jan. 2006.

[20] E. W. Andrews, G. Gioux, P. Onck, and L. J. Gibson, "Size effects in ductile cellular solids. Part II: experimental results," *Int. J. Mech. Sci.*, vol. 43, pp. 701–713, 2001.

[21] S. S. Al-Bermani, M. L. Blackmore, W. Zhang, and I. Todd, "The Origin of Microstructural Diversity, Texture, and Mechanical Properties in Electron Beam Melted Ti-6Al-4V," *Metall. Mater. Trans. A*, vol. 41, no. 13, pp. 3422–3434, Aug. 2010.

[22] Y. Sun, B. Amirrasouli, S. B. Razavi, Q. M. Li, T. Lowe, and P. J. Withers, "Unloading elastic modulus at different stages of compression of ductile and brittle closed-cell foams," *In press*.

[23] C. Gaillard, J. F. Despois, and A. Mortensen, "Processing of NaCl powders of controlled size and shape for the microstructural tailoring of aluminium foams," *Mater. Sci. Eng. A*, vol. 374, pp. 250–262, 2004.

[24] B. Y. Conde, J. Despois, R. Goodall, A. Marmottant, L. Salvo, C. S. Marchi, and A. Mortensen, "Replication Processing of Highly Porous Materials **," *Adv. Eng. Mater.*, vol. 8, no. 9, pp. 795–803, 2006.

[25] S. M. Gaytan, L. E. Murr, F. Medina, E. Martinez, M. I. Lopez, and R. B. Wicker, “Advanced metal powder based manufacturing of complex components by electron beam melting,” *Mater. Technol. Adv. Perform. Mater.*, vol. 24, no. 3, pp. 180–190, Sep. 2009.

[26] L. E. Murr, K. N. Amato, S. J. Li, Y. X. Tian, X. Y. Cheng, S. M. Gaytan, E. Martinez, P. W. Shindo, F. Medina, and R. B. Wicker, “Microstructure and mechanical properties of open-cellular biomaterials prototypes for total knee replacement implants fabricated by electron beam melting.,” *J. Mech. Behav. Biomed. Mater.*, vol. 4, no. 7, pp. 1396–411, Oct. 2011.

[27] M. F. Ashby, A. Evans, N. a. Fleck, L. J. Gibson, J. W. Hutchinson, and H. N. G. Wadley, *Metal foams. A design guide.* Butterworth-Heinemann, 2000.

[28] L. E. Murr, S. M. Gaytan, F. Medina, E. Martinez, J. L. Martinez, D. H. Hernandez, B. I. Machado, D. a. Ramirez, and R. B. Wicker, “Characterization of Ti–6Al–4V open cellular foams fabricated by additive manufacturing using electron beam melting,” *Mater. Sci. Eng. A*, vol. 527, no. 7–8, pp. 1861–1868, Mar. 2010.

[29] N. Tuncer, G. Arslan, E. Maire, and L. Salvo, “Influence of cell aspect ratio on architecture and compressive strength of titanium foams,” *Mater. Sci. Eng. A*, vol. 528, no. 24, pp. 7368–7374, Sep. 2011.

[30] R. Goodall, Y. Conde, R. Mulluer, S. Soubielle, E. Combaz, J. Despois, A. Marmottant, F. Diologent, L. Salvo, and A. Mortensen, “uniaxial deformation of

microcellular metals Model systems and simplified analysis.pdf," in *IUTAM Symposium on Mechanical Properties of Cellular Materials*, 2009, pp. 1–8.